Real-Time Observation of Photoinduced Adiabatic Electron Transfer in Strongly Coupled Dye/Semiconductor Colloidal Systems with a 6 fs Time Constant

Robert Huber,[†] Jacques-E. Moser,[‡] Michael Grätzel,[‡] and Josef Wachtveitl*,[†,§]

Lehrstuhl für BioMolekulare Optik, Oettingenstrasse 67, Ludwig-Maximilians-Universität München, 80538 München, Germany, and Laboratory for Photonics & Interfaces, Institute of Physical Chemistry, Ecole Polytechnique Fédérale de Lausanne, CH-1015 Lausanne, Switzerland

Electron transfer from organic dye molecules to semiconductor−colloidal systems is among the fastest reported charge-separation reactions. We present investigations on alizarin complexing the surface of TiO$_2$ semiconductor colloids in solution. Because of the very strong electronic coupling between the sensitizer and the semiconductor in the alizarin/TiO$_2$ system, very fast electron injection from the photoexcited dye to the conduction band of TiO$_2$ occurs. The real-time observation of the injection process is achieved by transient absorption spectroscopy using a 19-fs excitation pulse provided by a pump pulse from a noncollinear optical parametric amplifier and a probe pulse from a quasi-chirp-free supercontinuum. An injection time τ_{inj} of 6 fs can be unambiguously derived in three different ways from the experimental data: (i) analysis of individual transients at spectral positions without contributions from subsequent reactions (relaxation, recombination); (ii) global fitting procedure for 31 wavelengths over a wide spectral range; and (iii) calculation of the S* state and comparison to the "nonreactive" system alizarin/ZrO$_2$. The spectral signature of the 6-fs kinetic component can be assigned to electron transfer from the excited dye molecule to the TiO$_2$ colloid. Even for this strongly coupled system, we propose a localized excitation with a subsequent adiabatic electron transfer reaction that is, to our knowledge, the fastest electron-transfer reaction that has been directly measured by transient spectroscopy.

1. Introduction

Sensitization of wide band gap semiconductors by organic dye molecules is a well-established technique with widespread applications such as the photographic process, detoxification and purification of water,[1] and, recently, solar energy-to-electricity conversion.[2−9] Considerable physical interest in these dye/semiconductor systems surely arises from the special energetic situation, allowing ultrafast electron transfer from a system with discrete energy levels on the donor side into a contiuum of energy levels on the acceptor side. In our case, the elementary reaction can be written as

$$S + h\nu \rightarrow S^* \rightarrow S^+ + e^-_{surf}(TiO_2) \rightarrow S^+ + e^-_{CB}(TiO_2) \quad (1)$$

where the dye attached to the colloidal surface is excited from the ground state S to the excited state S*, which is energetically situated above the conduction-band edge of the semiconductor. The excited dye molecule (S*) then acts as an electron donor, and electron transfer to the surface states of the semiconductor and subsequently to the conduction band (e$_{cb}$) occurs.[10−29] The dye molecule remains as the cation S$^+$. The back reaction and charge recombination to the ground state of the dye depend on the solvent, the presence or absence of electrolytes, the morphology of TiO$_2$, and the amount of adsorbed cations on the semiconductor surface.[30] The time scales for the back reaction vary from subpicoseconds to milliseconds.[8−10,23,31−36] A detailed theoretical treatment of interfacial electron transfer is complicated because reliable molecular models for the interface are needed and the presence of surface states or structural inhomogeneities has to be considered. Only recently was reasonable agreement between experiment and theory reported for interfacial electron-transfer reactions.[37,38] Nevertheless, because of the special energetic situation of a continuous band of acceptor levels, an activationless electron transfer can be presumed (Figure 1). According to Marcus theory, the only remaining parameter determining the injection rate should be the electronic coupling matrix element $|V|^2$, representing the electronic overlap integral between the donor and acceptor states. In weakly coupled systems, injection times of 100 fs−10 ps were found.[10,22,23,27,39−41] In a system like alizarin/TiO$_2$, in which a charge-transfer complex is formed between the organics and surface metal ions and is characterized by a new electronic π−d transition,[10] it is not clear, however, if the surface complex dye sensitizer undergoes a localized excitation (S $\rightarrow$ S*) or if the excitation process itself transfers an electron from the HOMO of the dye molecule directly into the conduction band (Ti d-orbitals manifold) of the semiconductor. Here, we report the observation of an ultrafast electron transfer for this system on a sub-10-fs time scale and propose that the sequence of reaction steps as indicated in eq 1 is still valid in the strong-coupling case.

2. Experimental Section

Measurements were performed on samples containing alizarin adsorbed either onto TiO$_2$ or onto ZrO$_2$ colloids. The systems

---

* To whom correspondence should be addressed. E-mail: wveitl@theochem.uni-frankfurt.de.

† Ludwig-Maximilians-Universität München.

‡ Ecole Polytechnique Fédérale de Lausanne.

§ Present address: Institut für Physikalische und Theoretische Chemie, Marie-Curie-Strasse 11, Goethe Universität Frankfurt, 60439 Frankfurt am Main, Germany.
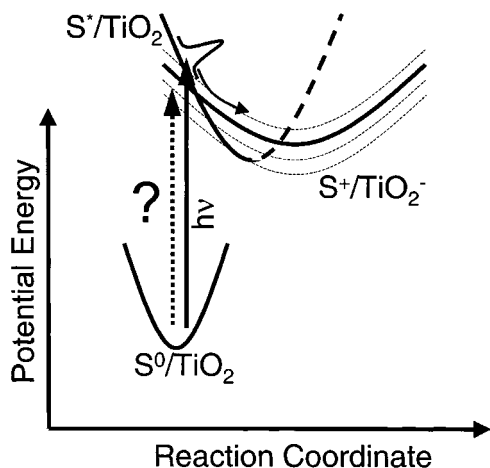
Electron Transfer in Dye/Semiconductor Systems

J. Phys. Chem. B, Vol. 106, No. 25, 2002 **6495**

Figure 1. Energetic scheme for the alizarin/TiO$_2$ electron-transfer reaction. The continuum of acceptor levels is represented by a series of vertically displaced parabolas. The photoexcitation of the dye could either lead to a direct injection of the electron into the TiO$_2$ conduction band (dotted vertical line) or to an electron-transfer reaction via the excited state of the dye S* (solid vertical line).

were diluted in methanol to final concentrations of 0.5 mM alizarin on 10 g/L TiO$_2$ colloids. The colloidal nanoparticles of TiO$_2$ were prepared as previously described via hydrolysis of TiCl$_4$ in cold water and further dialysis of the sol.[42] No stabilizing polymer was used. The average diameter of oxide particles was about 16 nm, as measured by dynamic light scattering.

ZrO$_2$ colloidal dispersions were prepared by hydrolysis of zirconium chloride in methanol. Ten grams of ZrCl$_4$ powder (Alfa) was dissolved in 150 mL of methanol. The solution was cooled to 0 °C and acidified by 0.5 mL of concentrated HCl, and 4 mL of H$_2$O was added. After 2 h of stirring at room temperature, the colloid was boiled under reflux for 2−3 h to favor crystallization of the oxide. The concentrated methanolic sol (150 mL) was finally diluted in pure water (700 mL) to yield a transparent colloid that typically contained 6 g/L ZrO$_2$ particles and ca. 18 vol % methanol. The hydrodynamic diameter of the ZrO$_2$ colloidal particles as determined by quasi-elastic light scattering was 10−20 nm.

For the transient absorption measurements, we used a classical pump/probe set up. The pump pulses (attenuated to 0.2 μJ at 495 nm) were provided by a noncollinear optical parametric amplifier (NOPA)[43] that was pumped with 50-μJ pulses at 400 nm of the second harmonic of a home-built Ti/sapphire regenerative amplifier system (1 kHz, 1 mJ, 800 nm). The NOPA was seeded with a white light supercontinuum that was generated in a calcium fluoride plate.[44] The resulting pulse-to-pulse energy fluctuations of the NOPA were less than 1% rms at fluctuations of <0.5% of the energy of the regenerative amplifier system at 800 nm. The pulse duration of the NOPA output after compression was measured by a home-built intensity autocorrelator (second harmonic generation in a 25-μm thick BBO) with material generating the same dispersion in the beam path from the NOPA to the autocorrelator as from the NOPA to the sample. The pulse compression of the NOPA pulses was performed by a standard prism compressor (SiO$_2$, 60°). The pulse duration of the compressed NOPA output was measured to be about 19 fs at a wavelength of 495 nm at the location of the sample. The diameter of the excitation spot inside the cuvette was 80 μm, and the optical path length through the sample was 50 μm.

The probe pulses were provided by supercontinuum (SC) generation in a CaF$_2$ plate with about 3 μJ of the 800-nm
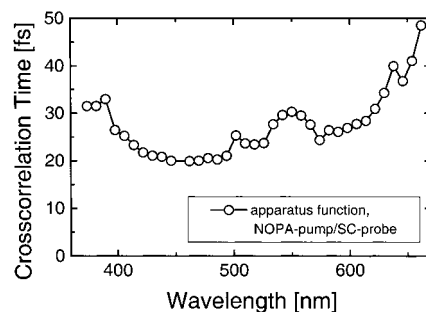

Figure 2. Cross-correlation time between the pump pulse and a probe pulse at a certain wavelength ($\Delta\lambda = 8$ nm) over the investigated spectral range.

fundamental of the regenerative amplifier. The low chirp of the SC generated in CaF$_2$ [44] (<25 fs^2 at 500 nm, <17 fs^2 at 700 nm) combined with a dispersion-reduced set up was the prerequisite for high temporal resolution. The SC is imaged via all reflective optics into the sample with a focal diameter of 40−50 μm, depending on the wavelength. The cross correlation functions, determined by fitting the coherent signals at the delay-time zeros,[45] were found to be in good agreement with measurements of two-photon absorption (see ref 46) and numerical summation of the following pulse-lengthening contributions : (a) the group velocity mismatch between the pump and probe pulses, (b) the chirp of the SC, and (c) the noncollinearity angle between the pump and probe (about 1° internal). As shown in Figure 2, the apparatus functions were 20−30 fs (fwhm) for 400 < λ/nm < 620 and <50 fs for the rest of the investigated wavelengths in the experiments reported here. The detection and data acquisition were performed as described in ref 47 and 48. By averaging about 4000 shots per scan and 16 scans per measurement, we were able to achieve a signal-to-noise ratio of up to 10^5 in transient transmission changes for the main part of the spectrum, depending on the opacity of the sample.

A precise determination of the delay-time zeros, which is the prerequisite for a reliable deconvolution of the measured transients, was realized in two independent ways: (a) the two-photon absorption signal, arising when pump and probe photons pass a long-pass filter glass simultaneously and (b) fitting the coherent signals at the delay-time zero that were recorded in pure methanol solution, as described in ref 45. In both cases, the determined delay-time zeros, varying with the probing wavelength, were fitted using the Sellmeier equation with the known amount of dispersive material in the beam path of the probing SC. This fitting procedure provides further reduction of the uncertainty in the specific delay-time zeros. The error can be estimated from the discrepancy between the measured values and the fit curve to be less than 2 fs. To detect a possible drift of the delay-time zeros with time, measurements of the sole solvent have been carried out before and after the measurement of the sample. This technique also allows us to identify identical temporal signatures of the transients caused by coherent effects at the delay-time zero in both the solvent and the sample. Thus, we were able to verify that the influence of the sample on the dispersion and consequently on the group velocity is negligible. A measurement of a colloidal solution of TiO$_2$ without alizarin has been carried out to analyze the potential signal originating from the sole colloids with regard to direct multiphoton interband excitation by the pump pulse. Besides the coherent signal at the delay-time zero, there were no further kinetic effects found. The pure-solvent data were used to subtract the electronic coherent signal at the delay-time zero.
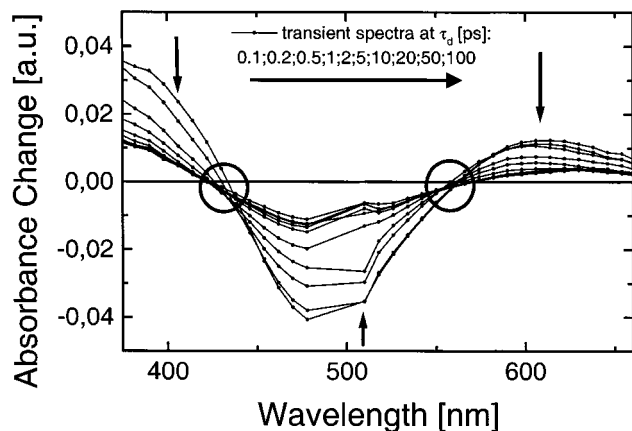
Figure 3. Transient difference spectra of alizarin on TiO$_2$. The isosbestic points at 426 and 570 nm (○) represent the spectral positions where the absorption of the alizarin cation and the absorption of the electron in the conduction band are equal to the ground-state absorption. The arrows indicate the direction of the transient spectra in the different spectral regions.

The analysis of the temporal evolution of the transient absorption spectra, especially the spectral assignment of the occurring transient species, was performed by a software package, developed at our institute, that supplies a fast Marquardt downhill algorithm for a global fit of the recorded data and simultaneously optimizes *n* global decay times for all of the recorded transients at once.

3. Results and Discussion

We present three different approaches for an unambiguous deconvolution of the transient signals to allow a thorough and reliable assignment of the observed time constants, especially the ultrafast sub-10-fs kinetic component. First, we concentrate on the transient absorbance changes at a spectral position where only the ultrafast kinetics occurs; the slower contributions cancel each other. Second, the complete set of data is analyzed by a global fitting procedure that optimizes an arbitrary number of decay times for all of the recorded transients at once. Third, the calculated excited-state spectra from the transient data show good agreement with the known excited-state spectra of the reference system alizarin on ZrO$_2$ and substantiate the reliability of the 6-fs component of the fitting procedure.

Deconvolution of a 6-fs Kinetic Component: Nonlinear Fit near the Isosbestic Point (λ_{pr} = 422 nm). Figure 3 shows transient spectra of alizarin complexing the surface of TiO$_2$ for different delay times after excitation with a 495-nm pulse. The spectral region for λ < 420 nm is dominated by the absorption of the alizarin cation, the region between 420 and 550 nm predominantly shows the influence of ground-state bleaching, and for λ > 600 nm, mainly the absorption of the injected electron can be seen. The spectral assignments are discussed in detail in ref 10. We showed that for the strongly coupled alizarin/TiO$_2$ system the transients for delay times >400 fs are already dominated by ground-state recombination, the primary reaction step of electron injection occurring much faster.[10] Therefore, the temporal evolution of the spectra shown in Figure 3 is primarily caused by ground-state relaxation:

$$S^+ + e^-_{cb}(TiO_2) \rightarrow S^0$$
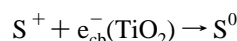
Only at ~422 and ~566 nm, where the sum of the absorbances of the electron in the conduction band (e$^-_{cb}$) and the dye cation (S$^+$) equals the ground-state absorption of alizarin (S^0) and
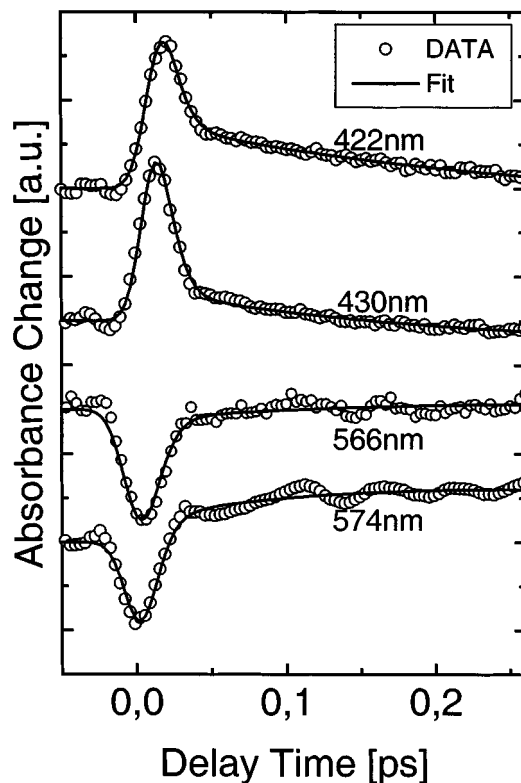

Figure 4. Transient absorbance changes around the two isosbestic points (○ in Figure 2). The transients show biphasic behavior. The first time constant is faster than the cross-correlation time. The second time constant is about 160 fs.

therefore the corresponding contributions cancel each other, can the isosbestic points for the back reactions be found. At the spectral position around 422 nm, there is no perfect isosbestic point, as can be seen in the transient spectra for 100 and 200 fs. But this small spectral difference does not hamper the analysis. This contribution will be described by a second time constant of 160 fs with a small amplitude. Figure 4 shows transients close to these two spectral positions where ultrafast biphasic absorbance changes can be clearly observed.

In the following section, we will describe the analysis for the single transient at 422 nm, which has a good signal-to-noise ratio and is not disturbed by coherent oscillatory components (such as e.g., the transient at 574 nm, bottom of Figure 4). Coherent effects and the observation of wave-packet motion accompanying the electron injection will be discussed in detail elsewhere.[49] The transient at 422 nm shows an initial increase in absorption followed by an ultrafast decrease. The observed subsequent ultrafast decay can be well approximated by fitting two exponential components with the following model function for the transient absorption $A(t)$

$$\Delta A(t) = \sum_{i=1}^{2} a_i(\tau_i) \exp\left(\frac{t_{cc}^2}{4\tau_i^2} - \frac{t - t_0}{\tau_i}\right) \frac{1 + erf\left(\frac{t - t_0}{t_{cc}} - \frac{t_{cc}}{2\tau_i}\right)}{2}$$

with the cross-correlation time t_{cc}, the delay time t, a delay constant t_0, the linear amplitudes a_i, the decay times τ_i, and the error function $erf(x)$ as the modeled apparatus function for a Gaussian-shaped cross-correlation function.

The second, longer decay time τ_2 with a time constant of 160 fs is obviously well-resolved with the temporal resolution of the set up.
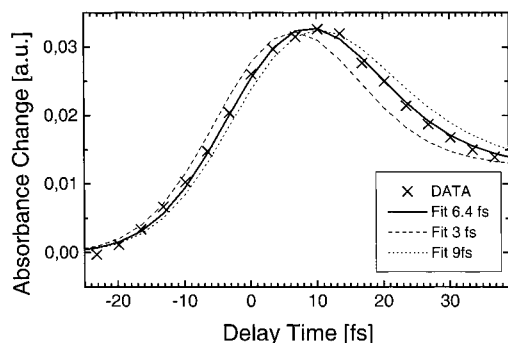
Figure 5. Exponential fit of the transient at 422 nm. The best fit results in a decay time of 6.4 fs (—). The results for decay times of 3 and 9 fs are shown as dashed (− − −) and dotted (···) lines, respectively.
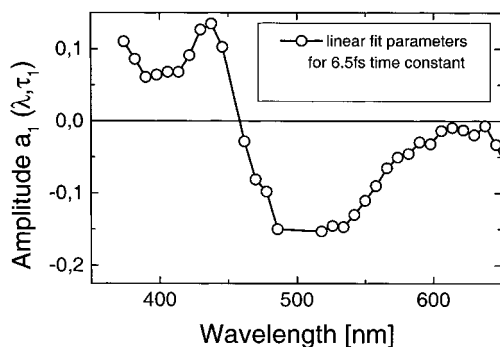

Figure 6. Amplitude spectra of the $\tau_1 = 6.5$-fs time constant derived from a global fitting procedure.

The best fit for the first, obviously much faster decay time τ_1 results in a time constant of 6.4 fs. To illustrate the mathematic reliability of the fit, Figure 5 shows fitting curves with different time constants; the dotted and the dashed curves are plots for a 3- and a 9-fs time constant. It can be well seen that there is a systematic discrepancy between the experimental data and the two fits. Therefore, the 3- and 9-fs time constants can be regarded as lower and upper limits, respectively, for the initial interfacial electron-transfer reaction. The robustness of the 6.4-fs value is supported by the fact that a variation of the initial start parameters for the nonlinear iterative fit results in deviations of the decay time below ±1 fs. It can be concluded that a fit at the spectral position located at the isosbestic point is numerically very stable and reliable, especially because the transient at 422 nm shows no pronounced perturbation by solvent effects at the delay-time zero and yields a time constant of 6.4 ± 1 fs.

Deconvolution of 6-fs Kinetics: Global Fitting Procedure. Because the visible pump/white light probe set up allows simultaneous acquisition of signals at multiple wavelengths, a complete set of data, recorded with high temporal resolution, was analyzed in a global fitting procedure. This set up also provides the possibility to investigate the existence of the ultrafast component in spectral regions where the sub-10-fs kinetic component is not as prominent as it is in the transients shown in Figure 4. Such a fitting algorithm is complicated by residual coherent signals but gives inherent evidence for the existence of the 6-fs component. The fitting procedure was performed with three time constants that were iteratively optimized, and decay times $\tau_1 = 6.5$ fs, $\tau_2 = 160$ fs, and $\tau_3 = 450$ fs were found. The time constant $\tau_1 = 6.5$ fs is in remarkably good agreement with the single fit of the 422-nm transient. The linear amplitudes are plotted in Figure 6, and the smooth shape of the spectrum indicates that the 6.5-fs time constant should be attributable to a real molecular species.

Physical Model for the Ultrafast Time Constant τ_1. The first situation to consider for a reaction model is whether the peak in the transient signal at 422 nm is really correlated with the electron injection reaction. In the following section, we will discuss and exclude possible effects causing artifacts.

Ultrafast transient absorption changes in this spectral region were observed neither for methanol nor for a colloidal TiO_2 solution without coupled alizarin. Furthermore, the coherent signal of the solvent around the delay-time zero was typically small and could be easily subtracted from the sample data.

Stimulated Raman processes could be envisioned as a possible reason for the observed ultrafast dynamics. If the frequency difference between the pump and the probe pulses corresponds to a vibrational transition of the solvent and if the pulses are shorter than the vibrational dephasing time T_2 of the solvent, then two peaks with different signs and with the characteristic bandwidth of the pump pulse should be visible in the transient absorption experiments (e.g., Raman gain at the low-frequency side and Raman loss at the high-frequency side of the pump pulse). The linear amplitudes of the global fitting procedure for the time constant τ_1 (Figure 6) indeed exhibits a significant positive peak at 438 nm, with an energy difference of 2629 cm^{-1} compared to the pump pulse (495 nm). However, because no prominent band is found in the spectrum of methanol and the corresponding negative peak at 569 nm is missing, stimulated Raman processes can be ruled out as the origin for the ultrafast dynamics.

Another possible origin for an ultrafast absorption signal could be two-photon absorption of a pump and a probe photon. However, the transients around the second isosbestic point at $\lambda = 566$ nm (Figure 4c and d) that show a negative transient difference absorbance with the same temporal evolution also allow us to exclude this effect.

Relaxation effects of the alizarin molecule such as internal vibrational redistribution and vibrational cooling or electron phonon scattering can be ruled out because they do not occur on these time scales. The relaxation of the hot, injected electron should also not occur on a time scale of <10 fs because of the empty conduction band of the semiconductor. Furthermore, none of these relaxation effects should give a signal with an amplitude comparable to the ground-state absorption of the alizarin.

The assignment of the recorded absorption signal to a real kinetic component that is caused by ultrafast electron injection following the photoexcitation appears, therefore, to be quite reasonable.

We propose the following model: The alizarin molecule is photoexcited into a localized electronic state S* that subsequently injects an electron into the TiO_2 colloid with a characteristic time of about 6 fs. The alizarin cation then undergoes an internal vibrational redistribution, and the electron moves from a surface state (with discrete energy levels) toward the colloidal bulk (with a continuous band structure). Analysis of the decay-related spectra provides a critical test of the proposed scenario.

Analysis of the Decay-Related Spectra. The global fitting procedure, which was performed for 31 different wavelengths, is in good agreement with the proposed model. As described above, the optimized global time constant is $\tau_1 = 6.5$ fs. The spectral signature of the linear parameter in Figure 6 for the decay time τ_1 can now be analyzed to assign the different species to components of the decay-associated spectrum. For comparison, the absorption spectra of the alizarin cation S^+, the alizarin ground-state S°, and the absorption of the electron in the colloid's conduction band are shown in Figure 7. For wave-

6498 *J. Phys. Chem. B, Vol. 106, No. 25, 2002*
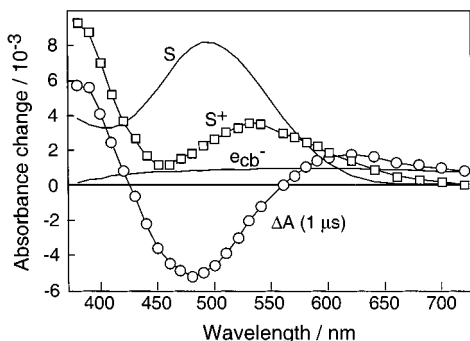
Huber et al.

Figure 7. Absorption spectra of alizarin, the alizarin cation, and the electron in the conduction band. The spectra of the cation and the electron in the conduction band were obtained by nanosecond spectroscopy, as described in ref 10.

Figure 8. Comparison of the excited-state spectra for the "nonreactive" (alizarin/ZrO$_2$; ○) and the reactive (alizarin/TiO$_2$; □) systems. The former spectrum was obtained from the transient spectrum at delay time $t_d = 50$ fs (corrected for ground-state bleaching), and the latter, from the spectrum obtained after deconvolution of the apparatus response function (at $t_d = 0$ fs).

lengths <460 nm, the decay-associated spectrum can be assigned to the cation formation and to the rise of absorption due to the injected electron (smaller amplitude). The pronounced minimum between 500 and 550 nm reflects the cation absorption (at systematically longer wavelengths than the ground state absorption), whereas the flat, unstructured region at $\lambda > 580$ nm is typical for the injected electron. The negative sign of the fit amplitudes observed in this spectral region ($\lambda > 475$ nm) is indicative of a rise in absorption (negative exponential decay) and further supports the model of the formation of the alizarin cation and an electron in the conduction band. The positive amplitudes for $\lambda < 460$ nm arise from the excited-state absorption, which is partially compensated for by $\lambda < 430$ nm, again in good agreement with the increasing absorption of S$^+$ in the spectrum for $\lambda < 450$ nm in Figure 7. In summary, the spectral characteristics of the fast time component τ_1 fit perfectly with an electron injection process for the complete range of wavelengths between 350 and 650 nm that reflects cation formation, the vanishing S* state, and the electron in the semiconductor colloid.

Other possible physical processes, such as ultrafast molecular reorganization with a dynamic shift in the spectral signatures, can also be excluded because they would result in a characteristic antisymmetric feature in the decay-related spectra, which was not found experimentally. Furthermore, ultrafast formation of the triplet state as observed in other dyes[50] can be ruled out for alizarin because transient femtosecond absorption measurements on the free dye in solution gave no indication of fast relaxation to the triplet state.[10]

Comparison of the Calculated S* Spectrum to the Reference System. The assignment of the instantaneous absorbance increase to excited-state absorption can be further confirmed by comparing the excited-state spectrum of alizarin on TiO$_2$ to the spectrum of alizarin on ZrO$_2$. We showed[10] that for this system the excited state of the alizarin is repopulated after 1 ps to about 80%. Consequently, the transient spectrum of alizarin adsorbed on ZrO$_2$ should look similar to the initial transient spectrum of alizarin on TiO$_2$ at delay time $t = 0$. Because of the fast decay of the excited state in the latter case, the transient spectrum at $t = 0$ has to be deconvoluted from the decay-related spectra. This deconvolution can be done by simply summing the linear fitting amplitudes for the different decay times for each channel of the global fit, resulting in the transient spectrum at delay-time zero that would be measured by a set up with infinite temporal resolution. From the transient spectra, the excited-state spectra are then calculated by subtraction of the ground-state contribution. However, this analysis does not take into account any initial spectral evolution of the S* spectrum
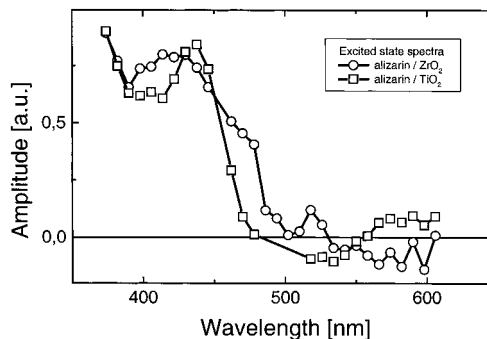
that might occur on this time scale; propagation of the initially generated wave packet on the S* potential energy surface could lead to a delayed onset of the S* absorption depending on the spectral position. This delay leads to a significant perturbation of the calculated excited-state spectrum, limiting the accuracy of the analysis. Furthermore, contributions of stimulated emission have also not been taken into account because significant fluorescence is observed only for $\lambda > 600$ nm. It should be mentioned that the spectra in Figure 8 give only a rough, qualitative indication of the involved species rather than perfect absorption characteristics, as evidenced, for example, by the nonphysical negative contributions for $\lambda > 575$ nm resulting from the imperfect subtraction process. Figure 8 shows both S* spectra for the systems alizarin/TiO$_2$ and alizarin/ZrO$_2$. The qualitative good agreement provides very strong evidence for the assignment of the 6-fs time constant to the decay of the excited-state S*. The spectral shape of the S* band is also broad enough to account for 6-fs kinetics with respect to the energy−time uncertainty.

As a consequence, we can assert that despite the strong electronic coupling in alizarin/TiO$_2$ there is no direct excitation into the conduction band of the colloid as indicated by the dashed arrow in Figure 1. The excitation process can be seen as a localized excitation of the dye molecule from the S° to the S* state and a subsequent injection into the colloid's conduction band.

Nevertheless, it should be pointed out that the application of rate constants within our fitting procedures, assuming an exponential population and decay of the S* and the S$^+$ states, is only a first, crude approximation to the correct description of this system but is certainly appropriate to give an idea of the relevant time scale of the charge injection process.

4. Conclusions

Even in the strongly coupled system alizarin/TiO$_2$, for which a large spectral shift in the absorption of the organic dye is due to complexation of surface Ti^{IV}ions, the nature of the absorption band still represents a localized S° → S^1 excitation with subsequent electron injection and cation radical formation and is not a direct charge-transfer absorption into the semiconductor conduction band (see Figure 1, dashed and solid arrows). The observed electron injection process is, to our knowledge, the fastest electron-transfer reaction ever directly observed by transient absorption spectroscopy identifying all involved species simultaneously. The measured 6-fs injection time correlates well with the expectation of an ultrafast electron transfer that is indicated by the strong electronic coupling matrix element.[10]

Electron Transfer in Dye/Semiconductor Systems

J. Phys. Chem. B, Vol. 106, No. 25, 2002 **6499**

References and Notes

(1) Wu, T.; Liu, G.; Zhao, J. *J. Phys. Chem.* **1999**, *103*, 4862.

(2) Hagfeldt, A.; Björksten, U.; Grätzel, M. *J. Phys. Chem.* **1996**, *100*, 8045.

(3) O'Regan, B.; Schwartz, D. T. *J. Appl. Phys.* **1996**, *80*, 4749.

(4) Bach, U.; Lupo, D.; Comte, P.; Moser, J. E.; Weissörtel, F.; Salbeck, J.; Spreitzer, H.; Grätzel, M. *Nature (London)* **1998**, *395*, 583.

(5) Enea, O.; Moser, J.; Grätzel, M. *J. Electroanal. Chem.* **1989**, *259*, 59.

(6) Nazeeruddin, M. K.; Kay, A.; Rodicio, I.; Humphry-Baker, R.; Müller, E.; Liska, P.; Vlachopoulos, N.; Grätzel, M. *J. Am. Chem. Soc.* **1993**, *115*, 6382.

(7) Nazeeruddin, M. K.; Liska, P.; Moser, J.; Vlachopoulos, N.; Grätzel, M. *Helv. Chim. Acta* **1990**, *73*, 1788.

(8) O'Regan, B.; Grätzel, M. *Nature (London)* **1991**, *353*, 737.

(9) O'Regan, B.; Moser, J.; Anderson, M.; Grätzel, M. *J. Phys. Chem.* **1990**, *94*, 8720.

(10) Huber, R.; Spörlein, S.; Moser, J. E.; Grätzel, M.; Wachtveitl, J. *J. Phys. Chem.* **2000**, *104*, 8995.

(11) Moser, J.; Grätzel, M.; Sharma, D. K.; Serpone, N. *Helv. Chim. Acta* **1985**, *24*, 1686.

(12) Moser, J.; Grätzel, M. *J. Am. Chem. Soc.* **1984**, *106*, 6557.

(13) Hilgendorff, M.; Sundström, V. *Chem. Phys. Lett.* **1998**, *287*, 5.

(14) Hilgendorff, M.; Sundström, V. *J. Phys. Chem. B* **1998**, *102*, 10505.

(15) Heimer, T. A.; Heilweil, E. J. *J. Phys. Chem.* **1997**, *101*, 10990.

(16) Ghosh, H. N.; Asbury, J. B.; Lian, T. *J. Phys. Chem.* **1998**, *102*, 6482.

(17) Ghosh, H. N.; Asbury, J. B.; Weng, Y.; Lian, T. *J. Phys. Chem.* **1998**, *102*, 10208.

(18) Tachibana, Y.; Moser, J. E.; Grätzel, M.; Klug, D. R.; Durrant, J. R. *J. Phys. Chem.* **1996**, *100*, 20056.

(19) Ellingson, R. J.; Asbury, J. B.; Ferrere, S.; Ghosh, H. N.; Sprague, J. R.; Lian, T.; Nozik, A. J. *J. Phys. Chem.* **1998**, *102*, 6455.

(20) Hannappel, T.; Burfeindt, B.; Storck, W. *J. Phys. Chem.* **1997**, *101*, 6799.

(21) Hannappel, T.; Zimmermann, C.; Meissner, B.; Burfeindt, B.; Storck, W.; Willig, F. *J. Phys. Chem.* **1998**, *102*, 3651.

(22) Burfeindt, B.; Hannappel, T.; Storck, W.; Willig, F. *J. Phys. Chem.* **1996**, *100*, 16463.

(23) Wachtveitl, J.; Huber, R.; Spörlein, S.; Moser, J. E.; Grätzel, M. *J. Photoenerg.* **1999**, *1*, 153.

(24) Kamat, P. V. *Prog. Reac. Kinet.* **1994**, *19*, 277.

(25) Argazzi, R.; Bignozzi, C. A.; Heimer, T. A.; Castellano, F. N.; Meyer, G. J. *J. Phys. Chem.* **1997**, *101*, 2591.

(26) Martini, I.; Hartland, G. V. *J. Phys. Chem.* **1996**, *100*, 19764.

(27) Martini, I.; Hodak, J. H.; Hartland, G. V. *J. Chem. Phys.* **1997**, *107*, 8064.

(28) Martini, I.; Hodak, J. H.; Hartland, G. V. *J. Phys. Chem.* **1998**, *102*, 607.

(29) Zimmermann, H.; Boyn, R. *Phys. Status Solidi B* **1987**, *139*, 533.

(30) Pelet, S.; Moser, J. E.; Grätzel, M. *J. Phys. Chem. B* **2000**, *104*, 1791.

(31) Nogueira, A. F.; De Paoli, M. A.; Montanari, I. *J. Phys. Chem. B* **2001**, *105*, 7517.

(32) Tachibana, Y.; Haque, S. A.; Mercer, I. P.; Moser, J. E.; Klug, D. R.; Durrant, J. R. *J. Phys. Chem. B* **2001**, *105*, 1089.

(33) Ramakrishna, G.; Ghosh, N. G. *J. Phys. Chem. B* **2001**, *105*, 7000.

(34) Moser, J. E. *Sol. Energy Mater. Sol. Cells* **1995**, *38*, 1.

(35) Moser, J. E.; Grätzel, M. *Chem. Phys.* **1993**, *176*, 493.

(36) Haque, S. A.; Tachibana, Y.; Klug, D. R.; Durrant, J. R. *J. Phys. Chem.* **1998**, *102*, 1754.

(37) Gao, Y. Q.; Georgievskii, Y.; Marcus, R. A. *J. Chem. Phys.* **2000**, *112*, 3358.

(38) Gao, Y. Q.; Marcus, R. A. *J. Chem. Phys.* **2000**, *113*, 6351.

(39) Asbury, J. B.; Hao, E.; Wang, Y.; Ghosh, H. N.; Lian, T. *J. Phys. Chem. B* **2001**, *105*, 4545.

(40) Huber, R.; Spörlein, S.; Moser, J. E.; Grätzel, M.; Wachtveitl, J. *Ultrafast Phenomena XII*; Elsaesser, T., Mukamel, S., Murnane, M. M., Scherer, N. F., Eds.; Springer: Berlin, 2000; p 456.

(41) Rehm, J. M.; McLendon, G. L.; Nagasawa, Y.; Yoshihara, K.; Moser, J.; Grätzel, M. *J. Phys. Chem.* **1996**, *100*, 9577.

(42) Moser, J. E.; Grätzel, M. *J. Am. Chem. Soc.* **1983**, *105*, 6547.

(43) Wilhelm, T.; Piel, J.; Riedle, E. *Opt. Lett.* **1997**, *22*, 1474, 1494.

(44) Huber, R.; Satzger, H.; Zinth, W.; Wachtveitl, J. *Opt. Commun.* **2001**, *194*, 443.

(45) Kovalenko, S. A.; Dobryakov, A. L.; Ruthmann, J.; Ernsting, N. P. *Phys. Rev. A* **1999**, *59*, 2369.

(46) Rasmusson, M.; Tarnovsky, A. N.; Akesson, E.; Sundstrom, V. *Chem. Phys. Lett.* **2001**, *335*, 201.

(47) Nägele, T.; Hoche, R.; Zinth, W.; Wachtveitl, J. *Chem. Phys. Lett.* **1997**, *272*, 489.

(48) Huber, H.; Meyer, M.; Nägele, T.; Hartl, I.; Scheer, H.; Zinth, W.; Wachtveitl, J. *Chem. Phys.* **1995**, *197*, 297.

(49) Huber, R.; Moser, J. E.; Grätzel, M.; Wachtveitl, J., to be submitted for publication.

(50) Yeh, A.; Shank, C. V.; McCusker, J. K. *Science (Washington, D.C.)* **2000**, *289*, 935.